ISSN 0031-918X, The Physics of Metals and Metallography, 2016, Vol. 117, No. 3, pp. 214–221. © Pleiades Publishing, Ltd., 2016.
Original Russian Text © I.V. Belyaev, V.E. Bazhenov, A.V. Moiseev, A.V. Kireev, 2016, published in Fizika Metallov i Metallovedenie, 2016, Vol. 117, No. 3, pp. 224–232.

ELECTRICAL AND MAGNETIC PROPERTIES

New Fe–Co–Ni–Cu–Al–Ti Alloy for Single-Crystal Permanent Magnets

I. V. Belyaev[a], V. E. Bazhenov[b], A. V. Moiseev[a], and A. V. Kireev[a]

[a]*Stoletovs' Vladimir State University, ul. Gor'kogo 87, Vladimir, 600000 Russia*

[b]*National University of Science and Technology MISIS, Leninskii pr. 4, 119049 Moscow, Russia*

e-mail: V.E.Bagenov@gmail.com

Received April 7, 2015; in final form, June 6, 2015

Abstract—A new alloy intended for single-crystal permanent magnets has been suggested. The new alloy has been designed based on the well-known Fe–Co–Ni–Cu–Al–Ti system and contains to 1 wt % Hf. The alloy demonstrates an enhanced potential ability for single-crystal forming in the course of unidirectional solidification of ingot. Single-crystal permanent magnets manufactured from this alloy are characterized by a high level of magnetic properties. When designing the new alloy, computer simulation of the phase composition and calculations of solidification parameters of complex metallic systems have been performed using the Thermo-Calc software and calculation and experimental procedures based on quantitative metallographic analysis of quenched structures. After the corresponding heat treatment, the content of high-magnetic phase in the alloy is 10% higher than that in available analogous alloys.

Keywords: permanent magnets, Thermo-Calc, magnetic phase, magnetic properties, GRF, growth restriction factor

DOI: 10.1134/S0031918X16010038

INTRODUCTION

Russian State Standard GOST 17809-72 recommends two compositions of hard magnetic alloys—YuNDKT5AA and YuNDK40T8AA—for manufacturing single-crystal permanent magnets. The chemical compositions of these alloys and the magnetic properties of permanent magnets manufactured from these alloys are given in Table 1. In practice, it is only the YuNDKT5AA alloy that is used to manufacture single-crystal permanent magnets. The YuNDK40T8AA alloy is rarely employed because of the absence of demand in industry. This is caused by the insufficiently high magnitudes of remanence B_r and maximum energy product $(BH)_{max}$, as well as difficulties in forming a perfect single-crystal structure in ingots of this alloy.

At present, the achieved level of magnetic properties of the single-crystal YuNDKT5AA permanent magnets is at the maximum. The magnetic properties are $B_r = 1.1$ T, $H_c = 120$ kA/m, and $(BH)_{max} = 88$ kJ/m^3 and exceed those regulated by the State Standard. The level of magnetic properties cannot be increased further using manufacturing procedures. At the same time, when designing special technical equipment in which mainly single-crystal permanent magnets are used, new higher requirements for magnetic and service properties of permanent magnets are imposed. In the present study, we solved the problem via designing a new YuNDKT5AA-based alloy for single-crystal permanent magnets.

It is known that the level of B_r and $(BH)_{max}$ characteristics of single-crystal YuNDKT-type permanent magnets depends mainly on the volume fraction of the strong magnetic α' phase in the alloy and the perfection of single-crystal structure of ingots grown for these magnets [1, 2]. The higher the content of the strong magnetic phase in the alloy, the higher the B_r

Table 1. Chemical composition and magnetic properties of YuNDKT5AA and YuNDK40T8AA permanent magnets (Russian State Standard GOST 17809-72)

Alloy	Element content, wt %						Magnetic properties		
	Co	Ni	Cu	Al	Ti	Fe	B_r, T	H_c, kA/m	$(BH)_{max}$, kJ/m^3
YuNDKT5AA	34.5–35.5	13.5–14.5	2.5–4.6	7.0–7.5	5.0–5.5	balance	1.05	115	80.0
YuNDK40T8AA	39.0–40.0	14.0–14.5	3.0–4.0	7.2–7.7	7.0–8.0	balance	0.90	145	64.0

and $(BH)_{max}$ characteristics of permanent magnets manufactured from these alloys can be reached. Because of this, when designing a new alloy, its components should be selected so that they ensure that the region of existence of the strong magnetic α' phase is widened and facilitate the formation of perfect single-crystal structure in ingots.

It was shown [3] that the solidification process of any alloy includes the simultaneous occurrence of two sequential processes. The first process is the diffusion decomposition of solidified liquid, which is accompanied by the formation of crystals with a nonequilibrium composition. The second process is the diffusion interaction of these crystals with the surrounding liquid, which results in the formation of additional amount of solid and increase in the total fraction of crystals. After the completion of the second process, the composition of crystals becomes equilibrium for a given temperature. The mass fraction of crystals formed at the expense of the diffusion decomposition is designated as M_{dec} (or f_S^{dec}). The mass fraction of crystals formed at the expense of diffusion interaction is designated as M_{int} (or f_S^{int}). In the present study, we use f_S^{dec} and f_S^{int}, respectively. For different alloys, the ratio of the f_S^{dec} and f_S^{int} fractions can differ; however, the sum of the f_S^{dec} and f_S^{int} fractions always equals unity.

It was shown in further studies [2, 4, 5] that f_S^{dec} and f_S^{int} are fundamental characteristics, which determine the potential ability of alloy for the formation of one or another crystal structure of ingot during its solidification. The higher f_S^{dec} and, therefore, the lower f_S^{int}, the higher the potential ability of the alloy for the formation of single-crystal or coarse grain structure of ingot. Vise versa, the lower f_S^{dec} and, therefore, the higher f_S^{int}, the more difficult the formation of single-crystal structure in an ingot and the easier the formation of refined grain structure.

The single-crystal forming ability of an alloy upon the unidirectional solidification of cast ingots can be also estimated in another way. Tiller et al. [6] suggested the use of the following expression as the stability criterion for the planar solidification front:

$$G/R = [mC_0(1-k)]/Dk. \quad (1)$$

where G is the temperature gradient at the solidification front, R is the growth rate, m is the slope of liquidus, C_0 is the alloy composition, k is the distribution coefficient, and D is the coefficient of diffusion. According to [7, 8], the stability condition of planar solidification front is given in the form of the two-sided inequality $G/R < [mC_0(1-k)]/Dk$.

It follows from Eq. (1) that the higher $[mC_0(1-k)]/k$, the higher the temperature gradient and the lower the growth rate R of crystal that should be used to ensure the planar solidification front. Therefore, the developed columnar or single-crystal structure can be easier formed in the alloy characterized by the lower $[mC_0(1-k)]/k$. Subsequently, the $[mC_0(1-k)]/k$ expression was used to estimate the effect of alloy composition on the grain size in ingots and was called the supercooling parameter P [9, 10]. In [11], a solidification model has been suggested that takes into account the effect of the alloy composition using the $1/X$ parameter which was later called the growth restriction factor (GRF). The authors of [2] believe that the grain size correlates with Q rather than [12], since P characterizes the maximum possible supercooling of the alloy, which as a rule cannot be achieved, whereas Q indicates the degree of supercooling developed at the beginning of the solidification process as follows:

$$Q = m(k-1)C_0. \quad (2)$$

To calculate Q for the multicomponent systems, it was suggested in [13] that the contribution of each j component be summed and expression $Q = \sum_j m_j(k_j - 1)C_{0_j}$ be used. It has been shown in a number of studies [14–16] that simply summing does not always yield adequate results. Equation (2) cannot be used with high contents of the second component and significant interactions between components [15].

It was shown in [13] that the Q magnitude is inversely proportional to variations of the solid fraction with temperature $df_S/dT = 1/Q$. Subsequently, the equation

$$Q = (\partial \Delta T/\partial f_S)_{f_S \to 0}. \quad (3)$$

was used in [14–16]. The aim of the present study is to design an alloy characterized by maximum f_S^{dec} and minimum Q, which will facilitate the single-crystal structure formation in the course of directional solidification of ingot, to improve the perfection of single-crystal structure, and to increase the magnetic properties of single-crystal permanent magnets.

To achieve this goal, we used the results of preliminary studies on the effect of individual elements on the position of critical points and the solidification behavior of YuNDKT-type alloys. In particular, the studies have allowed us to conclude that 1-wt % additions of Nd, Ta, and Hf to the YuNDKT5AA alloy must lead to a decrease in the generalized distribution coefficient (k_g) of the alloy and, therefore, to an increase in the f_S^{dec} value. The current work continues previous studies.

EXPERIMENTAL

Melting of Alloys, Casting of Ingots, and Single-Crystal Growth

Alloys were melted using carbonyl iron, which was purified by vacuum melting, K-0 electrolytic cobalt, N-0 cathode nickel, M0k cathode copper, A99 aluminum, iodide titanium, NbSh-1 niobium in the form of rods, and iodide hafnium. The melting was performed in an argon atmosphere using an ISV-0.016 vacuum induction furnace and a pure alumina crucible. During melting, to decrease the carbon content in the alloy to less than 0.03%, the melt was treated with a solid oxidizer. As the oxidizer, we used a Fe_2O_3 powder. The melt was cast into ceramic molds manufactured by the investment casting method. The surface of receiving and pouring cup, which contacts with the melt, was made from pure alumina. Polycrystalline cast ingots formed after the melt solidification subsequently were used for growing single crystals.

Each of the melted alloys was used to grow single crystals (ingots) 21 mm in diameter and 180 mm in length. The single crystals were grown in an argon atmosphere by Bridgman technique using a Kristallizator 203 installation. We used attested single-crystal seeds oriented along the ⟨100⟩ crystallographic direction and heat resistant corundum containers with titanium getter coating. The growth rate was 0.4 mm/min at the vertical temperature gradient at the solidification front of 100 K/s. The single-crystal structure perfection of ingots was estimated by metallographic analysis based on the presence or absence of spurious crystals in the structure and on the degree of block misorientation. Moreover, the single-crystal structure perfection was judged by the behavior of the magnetization reversal curves. It is known that the higher the single-crystal structure perfection of ingot, the higher the magnetic-hysteresis loop squareness for magnets manufactured from the ingot.

Permanent magnets were manufactured from all prepared single-crystal ingots. The ingots were cut into samples 21 mm in diameter and 10 mm in length, which were subjected to thermomagnetic treatment that includes the following stages: isothermal holding at 805 ± 1°C for 12 min in a magnetic field of 250 kA/m and tempering in a PKL-1.2-36 resistance furnace, which consists in the step-by-step holding at 680°C for 0.5 h, 650°C for 2 h, 580°C for 3 h, and 580°C for 5 h. After that, the samples were subjected to furnace cooling to room temperature. The magnetic properties of samples were estimated by the continuous recording of magnetization reversal curves using a PERMAGRAPH C-300 installation.

The chemical composition of melted alloys was determined using an ARL ADVANT'X (Thermo Scientific, United States) standard-free fluorescence spectrometer. The sulfur and carbon contents in the alloys were determined using an ELTRA CS-800 (Germany) analyzer.

The liquidus and solidus temperatures of the alloys were determined by differential thermal analysis (DTA) using a Setaram (France) installation.

The quantitative phase analysis was performed using a DRON-3 (Russia) and D8 Advance (Bruker AXS, Germany) diffractometers. X-ray diffraction patterns were taken using Co$K\alpha$ radiation and powders prepared from single-crystal ingots subjected to all isothermal heat treatments. The volume fractions of phases were determined by the automated calculation of pulses using a specific software.

Procedure for Calculating f_S^{dec} and Q by Thermo-Calc

To calculate the f_S^{dec} parameter with the Thermo-Calc software, we used the expression [2]

$$f_S^{dec} = \int_{T_S}^{T_L} -\frac{dC_L f_L}{C_L - C_S}. \quad (4)$$

where T_L and T_S are the liquidus and solidus temperatures of the alloys, respectively, and C_L and C_S are the compositions of the liquid and solid, respectively. The dependences $C_L = f(T)$ and $C_S = f(T)$ were obtained in the form of fourth-power polynomials using a regression technique. In this case, the phase composition of alloys was calculated for 20 temperatures in the temperature range between the liquidus and solidus temperatures using the Thermo-Calc software, the CALPHAD method, and SNOB3 thermodynamic database. The coefficient of determination R^2 for the dependences $C_L = f(T)$ and $C_S = f(T)$ is close to unity (>0.999).

The growth restriction factor Q was calculated using Thermo-Calc software by variations of the solid fraction with temperature. It is known that, at the start time, the differences between the equilibrium and nonequilibrium solidification processes are minimal. Therefore, we plot the dependences of the solid fraction on temperature for the equilibrium solidification. Equation (3) can be represented in the form of infinitesimal increments as follows:

$$\begin{aligned} Q &= d\Delta T/df_S = \Delta(\Delta T)/\Delta f_S \\ &= (\Delta T_2 - \Delta T_1)/(f_{S2} - f_{S1}). \end{aligned} \quad (5)$$

We used the constant value $f_{S2} = 0.1$ for all alloys. Since Q is calculated for temperatures close to the liquidus temperature and for $f_{S1} = 0$ and $\Delta T_1 = 0$ (Fig. 1), we have

$$Q = \Delta T_2/f_{S2}. \quad (6)$$

Estimating f_S^{dec} and Q Based on Experimental $f_S(T)$ Dependences

To determine the temperature dependence of the solid fraction $f_S(T)$, we used the metallographic analy-

sis of quenched structures. A studied sample 20–30 g in mass was placed into an alumina crucible. The temperature was measured with a PtRh30/6 thermocouple, which was preliminary calibrated for pure metal standards, such as aluminum, copper, and nickel. The crucible was placed on a free-falling plug located in the bottom of resistance furnace. The plug was fixed with a fixing device. A sample was heated to 1400°C and held at this temperature for ~10 min to attain complete melting and equalize the melt temperature. Then, the studied alloys were subjected to water quenching from various temperatures corresponding to the solidification range, which was preliminarily determined by DTA. Quantitative results of the metallographic analysis of quenched samples were used to plot experimental temperature dependences of the solid fraction within the solidification range. The plotted dependences $f_S(T)$ were approximated with a mathematical function. The differentiation of the function with respect to temperature allowed us to obtain the increment of solid fraction for any point within the solidification range, i.e., the solidification intensity (i) at this point. Further, the solidification intensity was determined for the liquidus and solidus. The procedure was elaborated using the binary Cu–10% Ni and Cu–7% Mn alloys, the phase diagrams of which are available and well understood. The content of solid in alloys at the quenching moment, which was determined by metallographic analysis using sections of the quenched samples, agree well with the data calculated from the Cu–Ni and Cu–Mn phase diagrams [17].

The distribution coefficient for binary systems k is the square root of the ratio i_S/i_L, $k = \sqrt{i_S/i_L}$ [4, 5]. Using the k values, f_S^{dec} for the alloy can be determined by expression [4]

$$f_S^{dec} = [k/(k-1)^2](1/k + \ln k - 1). \quad (7)$$

The quantity Q was calculated using the dependence $f_S(T)$ and the procedure applied in the case of calculations by the Thermo-Calc software (Fig. 1).

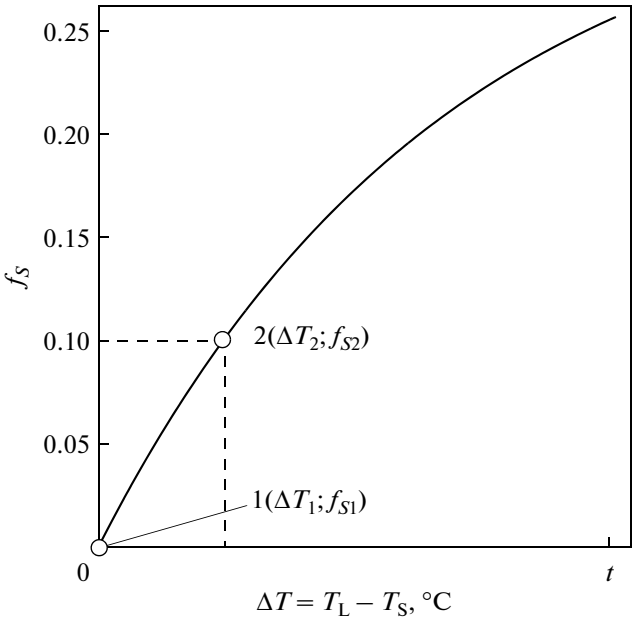

Fig. 1. Schematic diagram for calculating the GRF (Q).

RESULTS AND DISCUSSION

Calculation of f_S^{dec} and Q by Thermo-Calc Software

The YuNDKT5AA alloy (Table 1) was used as the base alloy. New alloys were prepared by introducing alloying elements that are substituted for iron in the base alloy. We have selected three elements, Nb, Ta, and Hf, the contents of which in the alloy are to 1.0 wt %. As was mentioned above, these elements were selected based on the results of preliminary studies. Table 2 shows the f_S^{dec} and Q values for the base YuNDKT5AA alloy and compositions with additions.

It can be seen from Table 2 that the Nb and Ta additions in the YuNDKT5AA alloy lead to a decrease in f_S^{dec} of the base alloy, whereas the addition of Hf leads to its increase f_S^{dec}. Calculations show that all these elements favor an increase of Q, but hafnium increases it to a lesser degree. Therefore, among all the studied elements, only hafnium favors the formation of a perfect single-crystal structure in the cast YuNDKT5AA ingots during their unidirectional solidification and, thus, achieving high magnetic properties of magnets manufactured from the ingots. It should be taken into account that f_S^{dec} and Q vary only slightly when Nb, Ta, and Hf are added. Results obtained for Ta and Nb are close; therefore, for the experiments, we used only one of them, namely, Nb.

Table 2. Magnitudes of f_S^{dec} and Q for the base YuNDKT5AA alloy (Fe–35.2% Co–14.3% Ni–7.1% Al–2.8% Cu–5.3% Ti) with Nb, Ta, and Hf additions calculated by Thermo-Calc software

Alloy	f_S^{dec}	Q
YuNDKT5AA	0.608	53.0
YuNDKT5AA + 1% Nb	0.606	53.8
YuNDKT5AA + 1% Ta	0.606	53.5
YuNDKT5AA + 1% Hf	0.611	53.4

Table 3. Chemical composition of the prepared YuNDKT5AA, YuNDKT5AA + 1% Nb, and YuNDKT5AA + 1 % Hf alloys and their liquidus and solidus temperatures

Alloy	Element content, wt %							T_L, °C	T_S, °C
	Co	Ni	Cu	Al	Ti	Nb(Hf)	Fe		
YuNDKT5AA	35.2	14.3	2.8	7.1	5.3	–	balance	1348	1272
YuNDKT5AA + 1% Nb	34.9	14.8	2.9	7.9	5.4	1.1	balance	1350	1270
YuNDKT5AA + 1% Hf	35.1	14.2	2.9	7.3	5.1	(0.8)	balance	1354	1268

Calculation of f_S^{dec} and Q from Experimental $f_S(T)$ Dependences

To experimentally confirm the efficiency of niobium and hafnium additions, we melted three alloys, i.e., the base YuNDKT5AA alloy and the YuNDKT5AA alloy with 1 wt % Nb and 1 wt % Hf.

Table 3 shows the compositions of the alloys and liquidus and solidus temperatures. As is seen we succeeded in preparing the alloys with the required niobium and hafnium contents.

Figure 2 shows the microstructure of the YuNDKT5AA + 1 wt % Nb alloy quenched in liquid state from different temperatures within the solidification range. Figure 3 shows the temperature dependences of the mass fraction of solid in the YuNDKT5AA, YuNDKT5AA + 1 wt % Nb, and YuNDKT5AA + 1 wt % Hf alloys quenched in liquid state from different temperatures, which were determined by metallographic analysis. Since the liquidus temperatures of the alloys are different, they were reduced to the unified scale by using the liquidus temperature as the zero temperature. The dependences were plotted on coordinates f_S–$(T_L - T)$. Figure 3 also shows the temperature dependences of the solid fraction, which were calculated by the Thermo-Calc software. The calculated dependences for all three alloys almost coincide and are indistinctive in Fig. 3.

The dependences $f_S(T_L - T)$ in the form of quadric polynomial (Fig. 4) were obtained by approximation of experimental dependences. As can be seen, the experimental temperature dependences of the solid fraction for the alloys under study are different. Table 4 shows the f_S^{dec} and Q values that were calculated using the experimental data.

As can be seen from Table 4, the presence of niobium and hafnium in the composition of the hard magnetic YuNDKT5AA alloy leads to an increase of f_S^{dec} and decrease of Q and, therefore, should lead to an increase in the ability of the alloy to form single crystals. The influence of hafnium is more efficient. Therefore, the hafnium additions most substantially favor the formation of a single-crystal structure in ingots manufactured under industrial conditions and the increase in magnetic properties of single-crystal permanent magnets. This conclusion can be inferred from the calculated data. Discrepancies between the calculated and experimental f_S^{dec} and Q values are slight and can result from experimental errors and

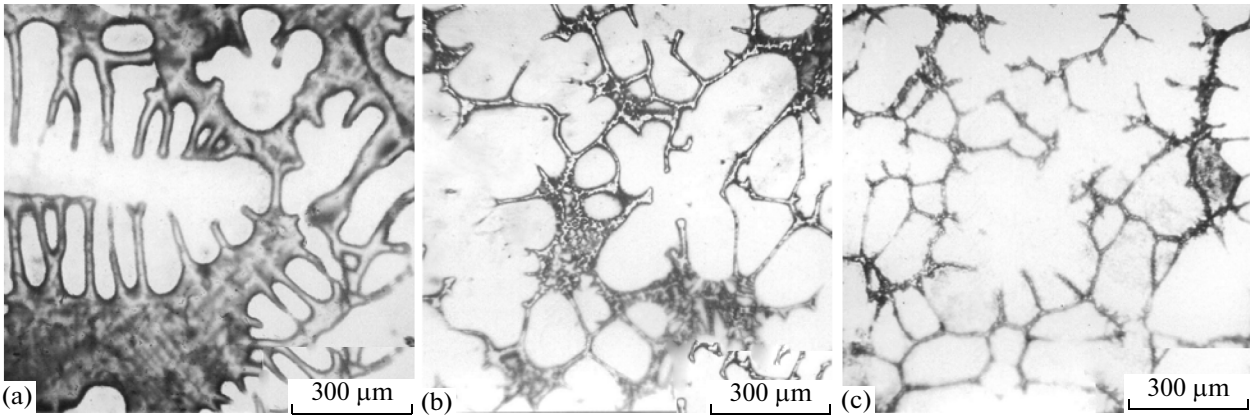

Fig. 2. Microstructure of the YuNDKT5AA + 1% Nb alloy quenched in liquid state from different temperatures within the solidification range: (a) $T_L - T = 20°C$; (b) $T_L - T = 50°C$; and (c) $T_L - T = 75°C$.

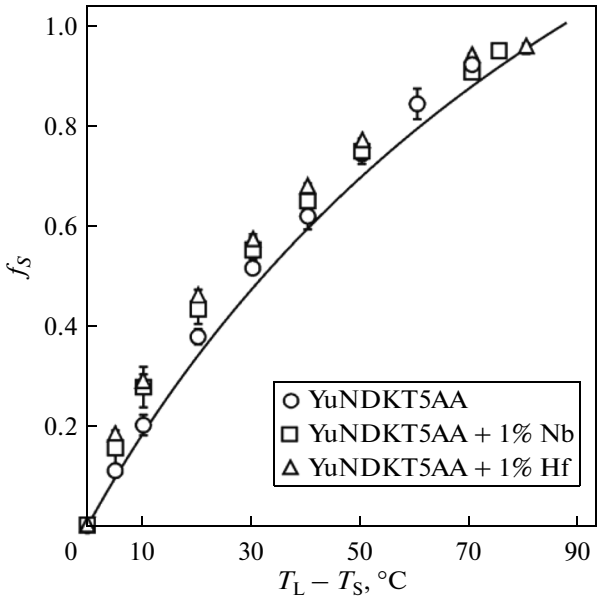

Fig. 3. Dependences of the solid fraction on the temperature $T_L - T$ determined by (△, □, ○) metallographic analysis of quenched in liquid state samples and (solid line) Thermo-Calc calculations.

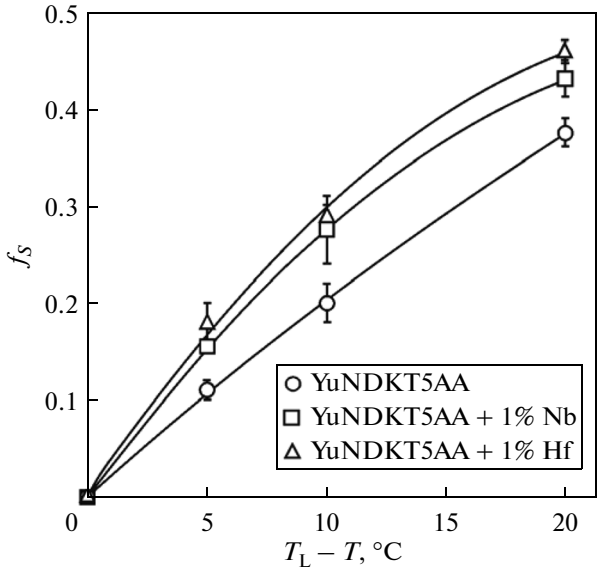

Fig. 4. Dependences of the solid fraction f_S on the temperature ($T_L - T$) for the alloys obtained by approximation of experimental data.

incomplete adequacy of the thermodynamic characteristics available in the used thermodynamic database. The SNOB3 database is common and contains 45 components and 389 phases. Since the experimental and calculated data indicate the more substantial effect of hafnium, no further experiments with the niobium-containing alloy were performed.

Casting of Ingots and Growth of Single-Crystals

Figure 5 shows the macrostructure of etched sections of the cast polycrystalline YuNDKT5AA and YuNDKT5AA + 1% Hf ingots.

It can be seen from Fig. 5 that the polycrystalline hafnium-containing ingots are characterized by coarser grains than those in the base alloy ingots. The average grain size of the base and hafnium-containing alloys, which was determined by the linear intercept method, is 1.24 ± 0.05 and 1.57 ± 0.08 mm, respectively. This fact indicates that the potential ability of the hafnium-containing alloy for the single-crystal formation in the course of directional solidification is higher than that for the base alloy.

Table 5 show the magnetic properties of single-crystal permanent magnets manufactured from the YuNDKT5AA and YuNDKT5AA + 1% Hf alloys (Table 3).

As is seen from Table 5, the 1-wt % hafnium addition to the base YuNDKT5AA alloy leads to the increase in the magnetic properties of single-crystal

Table 4. f_S^{dec} and Q for the YuNDKT5AA, YuNDKT5AA + 1% Nb, YuNDKT5AA + 1% Hf alloys calculated from experimental data

Alloy	k	f_S^{dec}	Q
YuNDKT5AA	0.68	0.564	47.7
YuNDKT5AA + 1% Nb	0.66	0.569	31.5
YuNDKT5AA + 1% Hf	0.60	0.587	29.2

Table 5. Magnetic properties of single-crystal permanent magnets prepared from the alloys studied (Table 3)

Alloy	B_r, T	H_c, kA/m	$(BH)_{max}$, kJ/m^3
YuNDKT5AA	1.057	118.9	84.6
YuNDKT5AA + 1% Hf	1.113	130.6	102.5

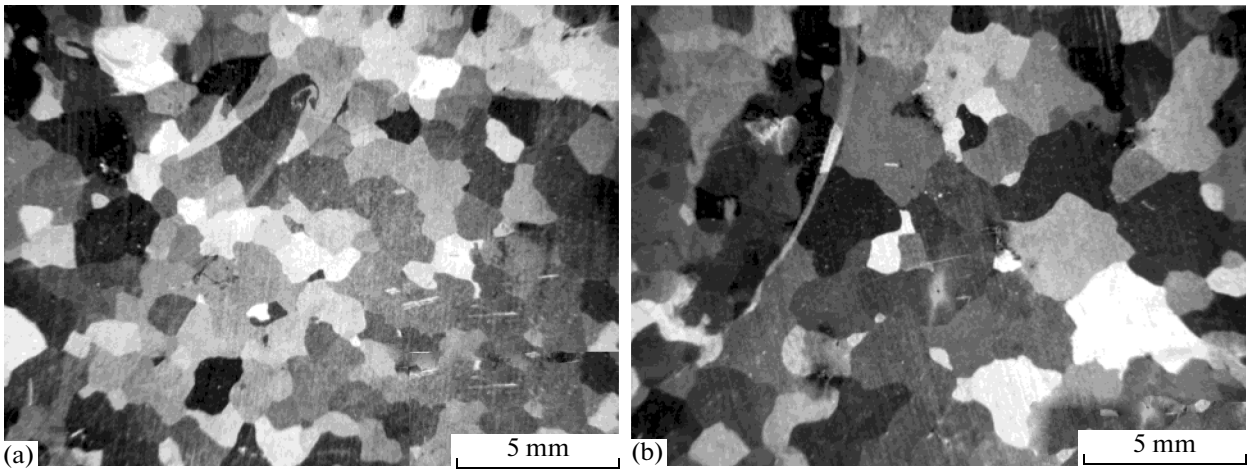

Fig. 5. Macrostructure of etched sections of cast ingots prepared from the (a) base YuNDKT5AA and (b) YuNDKT5AA + 1% Hf alloys.

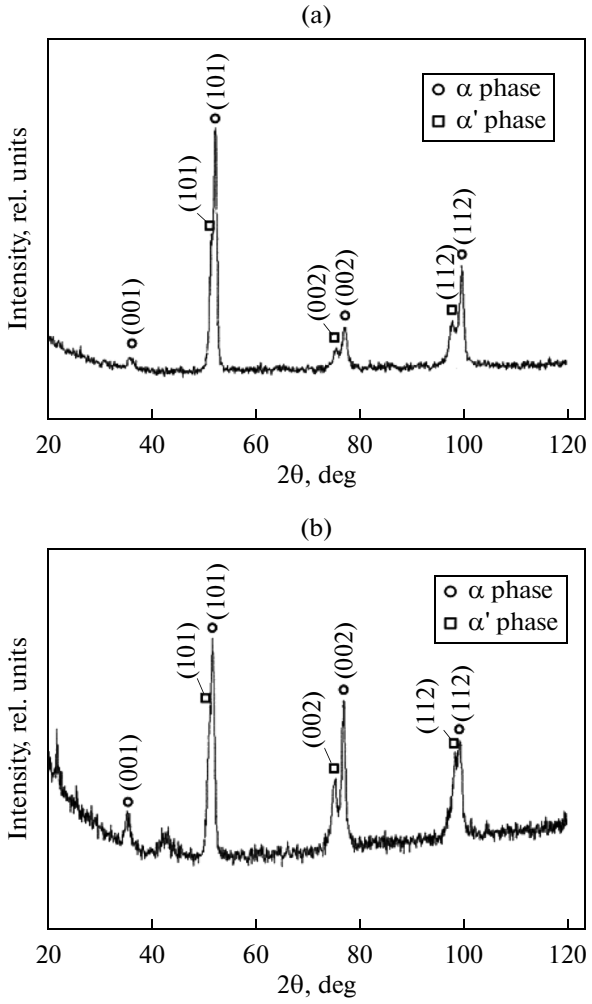

Fig. 6. X-ray diffraction patterns for the (a) base YuNDKT5AA and (b) YuNDKT5AA + 1% Hf alloys subjected to four-stage heat treatment.

permanent magnets. The remanence B_r demonstrates the almost 5% increase; the increase of H_{cb} and $(BH)_{max}$ is more than 10 and 20%, respectively.

To clarify the cause for the increase in the magnetic properties of the single-crystal hafnium-containing YuNDKT5AA permanent magnets, we studied the phase composition of the ingots. Figure 6 shows the results of the analysis. It follows from Fig. 6 that both alloys contain two α and α' phases. The both phases have a bcc structure and differ in the lattice parameter, which is 0.2885 and 0.2909 nm for the α and α' phase, respectively. According to the quantitative X-ray phase analysis, the volume fractions of the α and α' phases in the base YuNDKT5AA alloy subjected to all heat treatments are 70 and 30%, respectively. For the alloy containing 1% hafnium, the volume fractions of the phases are 60 and 40%, respectively. Thus, the hafnium addition results in an increase in the volume fraction of the high magnetic α' phase in the alloy; this fact is likely to be the cause for the increase in B_r and $(BH)_{max}$ of single-crystal permanent magnets prepared from the alloy.

The increase in B_r and $(BH)_{max}$ for the hafnium-containing magnets can be related also to the improved perfection of the single-crystal structure of prepared ingots. This fact is indicated by an increase in the squareness of the demagnetizing portion of hysteresis loop for the magnets manufactured from the ingots. Figure 7 shows the curves for the YuNDKT5AA and YuNDKT5AA + 1% Hf magnets.

The stimulus of the improvement of the single-crystal structure consists primarily in an increase of f_S^{dec} and decrease of Q for the YuNDT5AA alloy, which are due to the hafnium addition and lead to an increase in the ability to form a single crystal in an ingot in the course of its directional solidification; an increase in the alloy's ability allows one to prepare a highly perfect

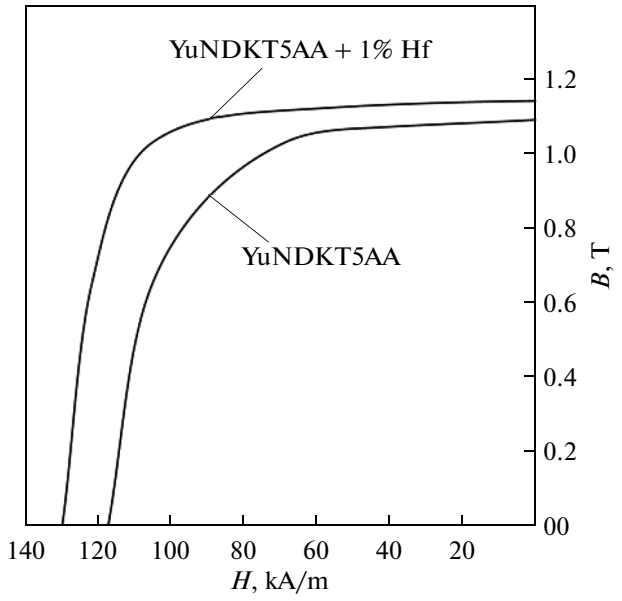

Fig. 7. Magnetization reversal curves for permanent magnets prepared from the YuNDKT5AA and YuNDKT5AA + 1% Hf alloys.

single-crystal structure under the same temperature and kinetic conditions.

The increase in the coercive force of the single-crystal hafnium-containing YuNDKT5AA permanent magnets is likely to be related to the effect of hafnium on the magnetic properties of the weak-magnetic α phase. The enrichment of the phase in hafnium is likely to decrease its saturation magnetization. Moreover, we may assume that the addition of hafnium to the alloy leads to an increase in the length-to-diameter ratio for a ferromagnetic particle, which is known to favor the increase in the coercive force [18].

CONCLUSIONS

The effect of Nb, Ta, and Hf additions on the solidification behavior of the YuNDKT5AA alloy was studied by the Thermo-Calc calculations and metallographic analysis of samples quenched in liquid state. The new YuNDKT5AA-based alloy with 1% Hf has been developed. The alloy is characterized by the higher f_S^{dec} magnitude and low GRF. This favors an increase in the ability of the alloy to form single crystals. The addition of hafnium likely leads to a broader range of existence of the weak-magnetic phase in the YuNDKT5AA alloy. Single-crystal permanent magnets prepared from the new alloy exhibit higher magnetic properties compared to those of single-crystal magnets prepared at present in accordance with the Russian State Standard GOST 7809-72.

REFERENCES

1. V. V. Sergeev and T. I. Bulygina, *Magnetoically Hard Materials* (Energiya, Moscow, 1980).
2. M. V. Pikunov, I. V. Belyaev, and E. V. Sidorov, *Crystallization of Alloys and Directional Solidification of Castings* (Vladimir. Gos. Univ., Vladimir, 2002) [in Russian].
3. M. V. Pikunov, "Analysis of the equilibrium crystallization of solid solutions," Izv. Vyssh. Uchebn. Zaved. Tsvetn. Metall., No. 5, 151–158 (1959).
4. M. V. Pikunov, I. V. Belyaev, and E. V. Sidorov, "On the calculation of thr crystallization coefficients of alloys–solid solutions," Izv. Vyssh. Uchebn. Zaved., Chern. Metall., No. 1, 121–124 (1998).
5. I. V. Belyaev, "Generalized segregation coefficient of multicomponent solid-solution alloys," Izv. Akad. Nauk., Met., No. 2, 106–108 (1998).
6. W. A. Tiller, K. A. Jackson, J. W. Rutter, and B. Chalmers, "The redistribution of solute atoms during the solidification of metals," Acta Metall. **1**, 428–437 (1953).
7. T. T. Cheng, "The mechanism of grain refinement in TiAl alloys by boron addition—An alternative hypothesis," Intermetallics **8**, 29–37 (2000).
8. Z. W. Huang, "Inhomogeneous microstructure in highly alloyed cast TiAl-based alloys, caused by microsegregation," Scr. Mater. **52**, 1021–1025 (2005).
9. L. A. Tarshis, J. L. Walker, and J. W. Rutter, "Experiments on the solidification structure of alloy castings," Metall. Trans. **2**, 2589–2597 (1971).
10. J. A. Spittle and S. Sadli, "Effect of alloy variables on grain refinement of binary aluminum alloys with Al–Ti–B," Mater. Sci. Techn. **11**, 533–537 (1995).
11. I. Maxwell and A. Hellawell, "Simple model for grain refinement during solidification," Acta Metall. **23**, 229–237 (1975).
12. A. L. Greer, A. M. Bunn, A. Tronche, P. V. Evans, and D. J. Bristow, "Modeling of inoculation of metallic melts: Application to grain refinement of aluminum by Al–Ti–B," Acta Mater. **48**, 2823–2835 (2000).
13. P. Desnain, Y. Fautrelle, J.-L. Meyer, J.-P. Riquet, and F. Durand, "Prediction of equiaxed grain density in multicomponent alloys, stirred electromagnetically," Acta Metall. Mater. **38**, 1513–1523 (1990).
14. M. A. Easton and D. H. St John, "A model of grain refinement incorporating alloy constitution and potency of heterogeneous nucleant particles," Acta Mater. **49**, 1867–1878 (2001).
15. T. E. Quested, A. T. Dinsdale, and A. L. Greer, "Thermodynamic modeling of growth-restriction effects in aluminum alloys," Acta Mater. **53**, 1323–1334 (2005).
16. R. Schmid-Fetzer and A. Kozlov, "Thermodynamic aspects of grain growth restriction in multicomponent alloy solidification," Acta Mater. **59**, 6133–6144 (2011).
17. M. V. Pikunov, I. V. Belyaev, and V. S. Lashuk, "Method of determination of ther intensity of alloy crystallization," Izv. Vyssh. Uchebn. Zaved, Chern. Metall., No. 9, 101–104 (1983).
18. I. B. Kekalo and B. A. Samarin, *Physical Metallurgy of Precision Alloys. Alloys with Special Magnetic Properties* (Metallurgiya, Moscow, 1989).

Translated by N. Kolchugina